X-ray photoelectron and Auger electron spectroscopy analysis of radio-frequency sputtered ultrathin films of amorphous carbon

W. Lu and K. Komvopoulos

Department of Mechanical Engineering, University of California, Berkeley, California 94720

Abstract

The compositions and carbon bonding structures of ultrathin carbon films deposited on Si(100) by radio frequency sputtering were analyzed by x-ray photoelectron spectroscopy (XPS) and x-ray Auger electron spectroscopy (XAES). The results indicate that the films consist of amorphous carbon (a-C) comprising both sp^2 and sp^3 hybridized carbon. From the analysis of the C 1s XPS spectra, the percentage of sp^3 carbon in a-C materials of films with nanohardness between 19 and 40 GPa was found to be in the range of 22-28%. XPS results show that energetic Ar^+ bombardment during film deposition promotes densification, removal of weakly bonded carbon and oxygen atoms from the film surface, and incorporation of Ar atoms, depending on the plasma environment in the vicinity of the growing film surface. The percentage of sp^3 carbon and the Ar content of the films increased with ion bombardment intensity. From the variations of the binding energy of core level Ar 2p electrons and the sp^3 carbon content with the Ar^+ bombardment intensity during film deposition, a stress-induced phase transformation from sp^2 to sp^3 carbon was determined for certain ion bombardment intensity. XAES analyses confirmed that the enhancement of the film nanohardness is due to densification, controlled by the intensity of energetic ion bombardment during film growth.

Submitted to the *Journal of Applied Physics* on June 28, 2001; revised manuscript submitted on January 3, 2002.

I. INTRODUCTION

Thin films of amorphous carbon (a-C) are widely used as protective overcoats in magnetic information storage, microelectronics, and optical communication technologies. Among the different deposition techniques for thin carbon films reviewed by Lifshitz,[1] filtered ion beam and cathodic arc are especially suitable for depositing high-quality tetrahedral a-C films with high contents of sp^3 carbon bonding. However, radio frequency (rf) sputtering is currently one of the most common techniques for high-volume, high-quality thin carbon film deposition and, as a result, has been used in various recent studies.[2-6] It is commonly accepted that the mechanical properties of a-C films (e.g., hardness) depend strongly on the film microstructure (e.g., atomic bonding, such as ratio of tetrahedral to trigonical carbon bonding, referred to as sp^3/sp^2), which is affected by the deposition conditions. Raman spectroscopy has been used to estimate the sp^2 and sp^3 carbon contents in sputtered a-C films[7] and to evaluate the residual stress in cathodic arc a-C films.[8]

Surface analysis techniques, such as x-ray photoelectron spectroscopy (XPS) and Auger electron spectroscopy (AES), have been used to study the composition and microstructure (especially the sp^2 and sp^3 hybridization in carbon materials) of thin a-C films synthesized by different methods. Contemporary XPS is a powerful surface analysis technique, which can provide both XPS and x-ray excited Auger electron spectroscopy (XAES) analyses of the very top surface layers. Photoelectrons from core levels excited by monochromatic x-ray can yield compositional information about the surface layer, chemical and mechanical environment of atoms in the near-surface region,[6,9,10] e.g., residual stress resulting from energetic ion bombardment during film growth, and atomic bonding of carbon materials.[4,11] Auger electrons in XAES analysis yield insight into the atomic bonding status of carbon films, such as contents of sp^3 and sp^2 carbon. Diaz et al.[11] estimated the sp^2 and sp^3 carbon fractions in

a-C films deposited on silicon substrates by pulsed laser evaporation of graphite targets by deconvoluting the core level C 1s XPS spectra. Their analysis was based on the fact that the components of the C 1s spectra at 284.3 and 285.2 eV can be related, respectively, to sp^2 and sp^3 carbon hybridizations. It was reported that the sp^3 carbon content in a-C films of hardness equal to 40 and 22 GPa was about 28.6% and 20%, respectively. Mizokawa et al.[12,13] used the peak-to-peak width of the main feature (measured from the most positive peak to the most negative peak of the main transition) in the first-order derivative of the carbon Auger spectrum obtained by XAES to investigate the composition of hydrogenated diamondlike carbon films deposited on silicon by dc sputtering. By studying the spectrum changes of the carbon films and a diamond surface in terms of the exposure time to ion bombardment, it was determined that energetic ion bombardment during sputtering produced carbon films rich in sp^2 hybridized carbon. Lascovich et al.[14,15] evaluated the sp^2/sp^3 ratio of pure and hydrogenated a-C films fabricated by dual ion beam sputtering by measuring the D value (i.e., the peak-to-peak width of the main transition mentioned earlier) in the first-order derivative XAES spectra and the binding energy shift of the C 1s XPS transition of the a-C films. For pure a-C films, the sp^2/sp^3 ratio was found to be equal to 3, revealing 25% sp^3 hybridization in the carbon materials.

The main objectives of this investigation were to use XPS and XAES techniques to study the compositions and bonding status (or microstructure) of ultrathin a-C films deposited on Si(100) substrates by rf sputtering, and to use the obtained information to elucidate the interdependence of the growth, microstructure, and nanomechanical properties of the films. The results and discussion in the following sections provide insight into the optimization of the deposition conditions of ultrathin a-C films with improved nanomechanical properties.

II. EXPERIMENTAL PROCEDURES

A. Deposition of carbon films

Thin a-C films of nominal thickness in the range of 10-70 nm were deposited on clean and smooth Si(100) substrates using a commercial rf sputtering system without magnetron. A high-purity graphite target and pure Ar gas were used for film deposition. The flow rate and working pressure of the Ar gas were fixed at 20 sccm and 3 mTorr, respectively. In all depositions, the base pressure in the chamber was less than 5×10^{-6} Torr. To obtain films with different microstructures and nanomechanical properties, the rf power P was set equal to 500 and 750 W, the substrate bias voltage V_S was varied between 0 and –300 V, and the deposition time t was fixed at 5 and 10 min. To provide a reference for both film thickness measurement and XPS/XAES surface analysis, the silicon substrates were partially masked during sputtering._Details about the rf sputtering system and deposition procedures can be found elsewhere.[5]

The deposition conditions and corresponding thickness d, root-mean-square surface roughness σ, effective hardness H_{eff}, and effective in-plane elastic modulus $[E/(1-\nu^2)]_{eff}$ of the a-C films examined in this study are given in Table I. An atomic force microscope (AFM, Nanoscope II, Digital Instruments) with a silicon tip of nominal radius of curvature equal to ~10 nm and a profilometer (Dektak IID, Veeco Instruments) with a vertical resolution of 0.5 nm were used to measure the surface roughness (from 1 μm × 1 μm surface area AFM images) and thickness of the a-C films, respectively. Hardness and elastic modulus values were obtained from nanoindentation experiments performed with a surface force microscope (SFM) consisting of an AFM retrofitted with a parallel-plate force transducer (Triboscope, Hysitron, Inc.). A diamond tip of nominal radius of curvature equal to ~20 nm and maximum contact load of 20 μN were used in all the indentation tests. The SFM and nanoindentation

procedures have been described in Refs. 4 and 5. The mechanical properties are referred to as "effective" due to the substrate effect. It has been reported[16] that the effect of the substrate compliance on the mechanical properties of ultrathin films measured by nanoindentation depends on the ratio of the contact depth h_c to the film thickness d. However, the small values of h_c/d given in Table I suggest that most of the measured nanomechanical properties (especially nanohardness) are fairly close to the true film properties.[16] Therefore, it is reasonable to correlate the measured effective nanohardness with the microstructure of the films.

B. XPS and XAES analysis of a-C films

The rf sputtered a-C films were characterized by XPS and XAES analyses using a Kratos Analytical XPS/XAES spectrometer with a monochromatic x-ray source of Al Kα ($h\nu$ = 1486.6 eV). XAES is an effective technique for atomic bonding analysis of radiation-sensitive material surfaces and ultrathin films. Conversely to conventional AES, surface damage due to energetic electron irradiation resulting in changes or even loss of some features of atomic bonding in carbon films[12,13] does not occur in XAES analysis. The samples were grouped in two separate batches (samples A-F and G-I in Table I). All samples of each batch were mounted on the same Cu sample holder using Ag colloid conductive paint, and were analyzed in the same run in order to facilitate the comparison of the results, especially binding energy and corresponding shift data. (Sample J was analyzed with other samples that were not examined in this study.) None of the samples was sputter cleaned by Ar^+ bombardment prior to the XPS/XAES analysis. The vacuum pressure during the XPS analysis was maintained in the range of 1-5 x 10^{-9} Torr. The spectrometer was operated at constant pass energy of 20 eV, an the analyzer resolution was equal to 2% of the pass energy. The XPS spectra of the C 1s transition were acquired at 0.1 eV energy steps. Pass energy of 50 eV and step energy of 0.2 eV were used to obtain the XAES

and XPS valence band spectra. Precautionary measures such as neutralizing the irradiated surface area with sufficient electrons and careful spectra processing were undertaken to avoid any charging effects during the XPS analysis. The x-ray illuminated spot size, defined by the Al Kα monochromator, was approximately 2 mm x 0.5 mm, i.e., the analyzed area was equal to ~1 mm^2. For comparison, XPS analysis was carried out on three different areas of each film surface and some silicon areas of the uncoated substrate region.

Elemental compositions of the a-C films were determined from the characteristic core level XPS spectra, using published sensitivity factors and assuming compositional uniformity throughout the film thickness. The microstructural constituents of carbon materials in the a-C films, i.e., sp^2 and sp^3 carbon fractions, were determined by decomposing the C 1s XPS spectra, after applying Shirley subtraction[17] for the inelastic scattering background and fitting Gaussian distributions at characteristic binding energies based on the method of Sherwood.[18] Since small amounts of O and N were detected on the film surfaces, six Gaussian distributions were fitted to the C 1s envelopes of the XPS spectra, as in a previous study of sputtered nitrogenated a-C films.[4] For the a-C films of this study, the full width at half magnitude (FWHM) of the six Gaussian distributions (each associated with a carbon constituent at a certain chemical state using characteristic binding energies in different environments)[11,19-22] was found to be between 1.2 and 1.7 eV.

For the integral XAES spectra of C KLL, three Gaussian distributions were used to fit the spectra after performing a 25-point Savinsky-Golay quadratic smoothing and a Shirley background subtraction.[17] Positions of these Gaussian peaks (i.e., the kinetic energies of the characteristic Auger electrons presented in binding energy scale) were determined based on this fitting method. The first-order derivative of the smoothed integral C KLL XAES spectra was obtained using a 25-point

Savinsky quadratic process. To avoid uncertainties, results from XAES analyses are given only for samples analyzed in the same run (samples A-F).

III. RESULTS AND DISCUSSION

A. Elemental compositions of a-C Films

Figure 1(a) shows the entire XPS spectrum of an a-C film (sample A), which is a representative spectrum of the films analyzed in this study. The spectrum includes the Auger transitions of C KLL (shown in Fig. 1(b) with three Gaussian fits in binding energy scale) and O KLL. Figure 1(c) shows the valence band XPS spectrum of this film. Peaks 1 and 3 in Fig. 1(c) correspond to Ar 3p and Ar 3s transitions, respectively, and peak 2 to C valence band transitions, which involve complicated XPS transitions due to the various states of C valence electrons in different hybridizations.[23,24] Table I gives information about the chemical composition of the films, determined from the measured relative intensities of characteristic peaks and sensitivity factors for certain elements in the XPS spectra. The values are averages of three measurements obtained from different areas of each sample. The presence of silicon is attributed to ion mixing of the film with the Si(100) substrate during deposition and/or possible local discontinuities in the film, such as pinholes.[6] The nitrogen content is due to adsorption of nitrogen on the freshly deposited carbon film surface, where dangling bond saturation occurred to lower the surface energy. After film deposition, nitrogen gas evaporated from liquid nitrogen was used to vent the chamber and cool down the samples. During this process, nitrogen was adsorbed (physically or even chemically) on the fresh carbon film surfaces, saturating some of the dangling bonds. The binding energy of N 1s was found to be in the very narrow range of 399.6-400.1 eV, compared to the N 1s binding energy of 401.4-402.5 eV obtained from the uncoated silicon surfaces of these samples. This is indicative of the formation of C-N bonds on the carbon film surfaces.[4,19-22] During venting, small

amounts of oxygen may be also introduced into the chamber from the liquid nitrogen source. In view of the very small amounts of silicon and nitrogen in the a-C films (Table I), it may be concluded that the significance of these elements on the film composition and mechanical properties is secondary. Thus, the presence of these elements will not be considered in the interpretation of the results presented in the following sections.

A1. Oxygen Content

The oxygen content of the a-C films may be attributed to contamination occurring during or after film deposition. Possible oxygen sources are residual water vapor in the working chamber, outgas of oxygen physically adsorbed on the chamber walls, silicon oxide layer present on the substrate surface before sputter cleaning, oxygen introduced in the chamber during nitrogen venting, and oxygen adsorbed on the film surfaces due to exposure to the atmosphere. Annealing experiments conducted in high vacuum demonstrated that the latter was the principal reason for the oxygen detected in the films. It was found that ~80% of the oxygen detected by XPS was due to adsorption of oxygen-containing air-born species from the ambient,[6] i.e., the oxygen in the a-C films after annealing at 495 ^{o}C for 85 min was less than ~2 at%. This indicates that the oxygen incorporated in the films during sputtering was in the range of 1-2 at%. The small amounts of oxygen in the bulk of the films suggest that film contamination during deposition was minimal.

Figure 2 shows the effect of rf power and substrate biasing on the oxygen content of a-C films deposited in 5 min. While the power effect is secondary, applying a substrate bias voltage of –200 V reduced the oxygen content by ~3 at%. This is attributed to energetic Ar^+ ion bombardment during film growth resulting in sputter etching of weakly bonded oxygen atoms on the growing carbon film surface. Another plausible reason for the differences in the oxygen content of the films is the densification caused

by ion bombardment. The greater porosity of the carbon films deposited under negligible ion bombardment (i.e., zero bias voltage) enhances oxygen adsorption and diffusion in the films. Hence, the different oxygen contents of the films deposited at power equal to 750 and 500 W and zero bias voltage (samples B and E, respectively) may be associated with the higher deposition rate at 750 W (Table I) that increased the film porosity (sample B). The lower oxygen contents obtained with substrate biasing can be related to the adsorbing-etching (resputtering) process encountered during film deposition. Despite the similar energies of C-O and C-C bonds, the sputter yield of oxygen due to Ar^+ bombardment is greater than that of carbon.[25,26] Thus, oxygen atoms adsorbing on the carbon film surface are sputtered off by bombarding Ar^+ ions much more easily than carbon atoms. Sputtering at 750 W power without substrate biasing yields a higher oxygen content, presumably due to more oxygen outgased from the chamber walls as a result of the increased heating and/or energetic particle bombardment at this high power. Comparison of the oxygen contents of the films deposited under identical conditions (Table I) shows that increasing the deposition time from 5 to 10 min resulted in negligibly small changes of the oxygen content in the carbon films.

A2. Argon Content

The argon content of the a-C films may be attributed to incorporation and/or implantation of Ar^+ ions during deposition, with implantation being the most dominant mechanism in the case of substrate biasing. Thus for fixed Ar pressure (equal to the working pressure in this study), the argon concentration in the carbon films depends on the power, substrate bias, deposition rate, and deposition time because these parameters control the incorporation and implantation of Ar during film growth. Substrate biasing causes Ar^+ ions to accelerate through the plasma sheath and bombard the film surface. Some of these energetic Ar^+ ions may be implanted into the growing carbon film. Consequently, the amount of

implanted Ar increases with the ion current density, which for low-pressure rf Ar discharges and fixed working pressure is approximately proportional only to the power,[5] and the kinetic energy of Ar^+ ions bombarding the film surface. Figure 3 shows the dependence of the Ar content on substrate bias voltage for 500 and 750 W power and deposition time equal to 5 min. The trend of the Ar content to increase with increasing absolute magnitude of bias voltage (i.e., increasing Ar^+ ion bombardment intensity) is in agreement with the previous interpretations.

In the absence of substrate biasing during film growth, the Ar^+ ions accelerate through the floating plasma sheath potential, bombarding the film surface at kinetic energy of ~10 eV.[25-27] At such low kinetic energy, the amount of Ar incorporated in the film is controlled by the fluxes of incoming carbon atoms (i.e., deposition rate) and Ar^+ ions (i.e., ion current density). Since most of the Ar atoms adsorbing on the growing film surface are quickly removed either by bombarding energetic particles or by evaporation, their dwell time on the film surface is very short. Thus the sticking coefficient of Ar is very low and exhibits a high sensitivity to the surface temperature. Considering the Ar concentrations of samples B and E and corresponding film thickness (Fig. 3 and Table I), less Ar was incorporated in sample B despite the higher fluxes of incoming Ar^+ ions and carbon atoms produced by the higher power.[5] This contradiction is attributed to the higher surface temperature of sample B during film growth due to the higher ion current density of bombarding ions at 10 eV, as evidenced by the markedly different surface roughness of the two films (Table I).

Figure 4 shows the dependence of the Ar content on the power and deposition time of the a-C films deposited under a bias voltage of –200 V. Due to the nonlinear film growth rate,[25-27] it is appropriate to examine the deposition time effect in terms of the amount of Ar incorporated in the films rather than the Ar content. Taking into account both the Ar concentration and the thickness of the films

deposited in 10 min (samples F and D), the amount of Ar in the film deposited at power of 750 W is greater than that in the film deposited at power of 500 W by ~34%, despite the higher Ar concentration obtained at a power of 500 W (Table I).

From the previous discussion about the Ar content in the a-C films, it is apparent that the Ar content depends on the intensity of Ar^+ ion bombardment during film growth and the flux ratio of incoming carbon atoms and energetic Ar^+ ions, which is important to the film density and mechanical properties.[2,5] Figure 5(a) shows the a-C film nanohardness as a function of Ar content. The film hardness increases with the Ar content up to ~1.9 at% and subsequently decreases abruptly. However, it is not likely that such very small amounts of Ar can produce such a pronounced effect on the film hardness. The reason for the hardening effect is the energetic Ar^+ ion bombardment during film deposition. The film with the highest Ar content (sample G) and lowest hardness in Fig. 5(a) was deposited in 5 min under a power of 750 W and bias voltage of –300 V. As discussed previously,[5] at 300 eV ion kinetic energy, Ar^+ irradiation damage degrades both the density and the hardness of the films. This is because migration and rearrangement of carbon atoms in the growing film due to thermal spikes becomes more dominant than knock-on (recoil) implantation,[28] which enhances film densification during deposition. Therefore, if there is a dispersion hardening effect of the embedded Ar atoms in the a-C films, its effectiveness depends primarily on the microstructure of the host a-C materials, which is controlled by the energetic Ar^+ ion bombardment during deposition.

B. Binding energies of Ar 2p, Ar 3s, and Ar 3p transitions

Although the Ar content hardly affects the hardness and elastic modulus of rf sputtered a-C films, as discussed above and reported in Ref. 2, small amounts of Ar in the films provide information about the plasma environment in which the films were synthesized[4] and the residual stress in the films,[6,9]

which is related to the binding energy shift of the Ar $2p_{3/2}$ XPS transition. Binding energy and FWHM data of Ar $2p_{3/2}$ XPS transitions for different a-C films are given in Table II. The binding energy is between 241.3 and 242.1 eV and the FWHM is in the narrow range of 1.01-1.06 eV, which reflects the inertness of the Ar atoms in the carbon films. The data indicate that energetic ion bombardment (substrate biasing) during film deposition causes the binding energy of Ar $2p_{3/2}$ to shift to lower values. This shift is attributed to the compressive residual stress in the a-C films introduced by the ion bombardment.[6,9]

Figure 5(b) shows the variation of the film nanohardness with binding energy of Ar $2p_{3/2}$ electrons. Hard films exhibit low binding energy of Ar $2p_{3/2}$. Among the a-C films examined, the hardest film (sample A) has a binding energy of 241.5 eV. However, two relatively softer films (samples D and C) demonstrated even lower binding energies, i.e., higher compressive stresses. This finding suggests that the highest film hardness does not necessarily correspond to the highest compressive residual stress.

Figures 6(a), 6(b), and 6(c) show the Ar 2p, Ar 3s, and Ar 3p XPS spectra, respectively, of different a-C films. Corresponding binding energy values are given in Table II. As shown in Fig. 6(a) and Table II, the FWHM values of the core level XPS transition Ar $2p_{3/2}$ of all the a-C films are very close. However, the shapes of the valence band XPS transition Ar 3p [Fig. 6(c)] are different, and energetic ion bombardment appears to have broadened the Ar 3p peaks. (FWHM values were not obtained for the valence band transitions.) It is also obvious that ion bombardment during deposition shifted the XPS peaks of both core level and valence band transitions. The binding energies of the valence band transitions Ar 3p and Ar 3s and the core level transition Ar $2p_{3/2}$ are in the ranges of 9.21-9.65, 22.35-22.93, and 241.3-242.1 eV, respectively (Table II). A comparison with the corresponding values[29] of pure free Ar (i.e., 13.6, 26.6, and 246.6 eV, respectively) shows that the binding energies of

the three Ar transitions decreased by about 3.7-5.3 eV when the Ar atoms were incorporated in the a-C films. This kind of binding energy shift is referred to as the matrix shift.[10] Figure 7(a) shows the binding energy shifts of the three Ar XPS transitions of different a-C films referred to those of free Ar atoms. The matrix shifts of the different XPS transitions of Ar in each film are not the same. Figure 7(b) shows a comparison of the binding energy shifts of the three Ar XPS transitions referred to those of sample B. These shifts are attributed to the compressive residual stress in the a-C films. According to the analysis of Ref. 9, the binding energy shifts of Ar 2p, Ar 3p, and Ar 3s transitions due to a given compressive stress should be the same. As shown in Fig. 7(b), the difference in the stress-induced shifts of the three Ar XPS transitions is in the range of 0.15-0.37 eV. Further investigation is required to clarify whether the different stress-induced shifts are due to different matrix shifts in each a-C film.

C. Analysis of XPS C 1s transition

Binding energy data of the core level XPS C 1s transition and corresponding FWHM values are given in Table II for different a-C films. The binding energy assumes values in the range of 284.3-284.5 eV, exhibits a long tail in the high-energy end of the spectrum, and the FWHM is in the range of 1.46-1.68 eV. These results indicate that the films possess different microstructures of a-C materials that depend on the deposition conditions. The binding energy and FWHM data for C 1s given in Table II suggest that energetic Ar^+ ion bombardment yielded a slight downward shift and broadening of the XPS C 1s peak, where peak broadening is attributed to amorphization.

Figure 8 shows a representative C 1s XPS spectrum of an a-C film (sample A). Since the films contain N (~1 at%) and O (~7 at%), six Gaussian fits corresponding to six characteristic C bonding statuses were fitted to the C 1s spectrum. The binding energies of these Gaussian fits [denoted by C 1s(1)-C 1s(6) in Table III and 1-6 in Fig. 8] are approximately equal to 284.4, 285.4, 286.7, 288.2,

289.9, and 291.7 eV. These binding energy values are correlated to different carbon bonding states,[4,23-26] i.e., C 1s(1): *sp*^{2} carbon; C 1s(2): *sp*^{3} carbon; C 1s(3): *sp*^{2} carbon with neighboring N atoms; C 1s(4): *sp*^{3} for carbon with neighboring N atoms; C 1s(5): *sp*^{2} carbon with neighboring O and N atoms; and C 1s(6): *sp*^{3} carbon with neighboring O and N atoms. Characteristic binding energies and corresponding atomic percentages for samples A-F are given in Table III. Based on these data, the percentage of *sp*^{3} carbon in the a-C materials of the films was calculated and is listed in Table III. Thus the *sp*^{3} hybridized carbon in the a-C films of this study is approximately 22-28% of the total carbon material. This percentage is in good agreement with the findings of other studies of similar sputtered a-C films.[4,11,14,15]

Figure 9 shows the variation of the binding energy of Ar $2p_{3/2}$ and the *sp*^{3} content in the a-C materials of the films with the Ar concentration. The *sp*^{3} fraction increases proportionally with the Ar content, affected by the energetic ion bombardment intensity during deposition and the flux ratio of carbon atoms and Ar^+ ions (Sec. IIIA2). This relation between the *sp*^{3} and Ar contents implies that energetic ion bombardment during deposition promotes the formation of *sp*^{3} carbon. As shown in Fig. 9, the binding energy of Ar $2p_{3/2}$ decreases with increasing Ar content in the range of 0-1.5 at%; however, for higher Ar contents, the binding energy increases, suggesting the occurrence of stress relaxation despite the higher ion bombardment intensity. For ~1.5 at% Ar, the biaxial compressive residual stress is predicted to be equal to 12-14 GPa,[9] which is close to the maximum compressive residual stress of 16 GPa reported in Ref. 2. The stress relaxation for Ar contents greater than ~1.5 at% and the continuous increase of the percentage of *sp*^{3} carbon reveal a stress-induced phase transformation from *sp*^{2} to *sp*^{3} carbon in the highly stressed a-C materials at a critical compressive stress of about -14 GPa. This kind of stress-induced phase transformation, where a very high compressive

stress forces pairs of sp^2 carbon sites to bond together to form sp^3 carbon configurations, was suggested by Schwan et al.[2] to interpret material densification by energetic Ar^+ ion bombardment during deposition and has been also observed in an annealing experiment of highly stressed sputtered a-C films.[6] Therefore, the increase of the sp^3 percentage and the development of a maximum compressive residual stress with increasing intensity of energetic ion bombardment can be attributed to a stress-induced phase transformation from sp^2 to sp^3 carbon. In addition, as evidenced from Fig. 10, the film nanohardness increases with the sp^3 percentage in the a-C materials. According to the discussion of the trends shown in Fig. 9, the increase of the intensity of energetic ion bombardment during film deposition enhances the formation of sp^3 carbon and promotes the densification of the carbon films. Therefore, the hardness increases due to film densification by ion bombardment, without necessarily the increase of the compressive residual stress.

D. XAES analysis

Figure 11 shows the first-order derivative $dN(E)/dE$ XAES spectra of two a-C films (samples A and B) with similar integral XAES spectra, such as that shown in Fig. 1(b). The $dN(E)/dE$ XAES spectrum contains three characteristic peaks. Based on the decomposition of the integral C KLL XAES spectrum [Fig. 1(b)] with three Gaussian fits after Shirley background subtraction, the kinetic energy KE and FWHM of the three features in the Auger spectra were calculated and are listed in Table IV, along with the kinetic energy difference ΔE between the first two transitions [peaks 1 and 2 in Fig. 1(b)] of the a-C films. The main peak is identified as the C KLL Auger peak with kinetic energy between 263.93 and 264.74 eV and FWHM values in the range of 19.23-19.83 eV. The kinetic energy of C KLL Auger electron for diamond and graphite is 262 and 268 eV, respectively.[12] In the $dN(E)/dE$ XAES spectrum, the width of the first main Auger peak, denoted as the D value (Fig. 11), measured from the

minimum to the maximum of the first main peak in the first-order derivative spectrum, can be used to calculate the sp^2/sp^3 ratio, based on the fact that the D value for diamond and graphite is equal to 14.3 and 22.5 eV, respectively.[14,15] The measured D values for the a-C films of this study were found to be in the range of 16.03-17.4 eV, i.e., closer to the D values of diamond.

The third main peak can be clearly identified as the Ar LMM Auger peak. Instead of obtaining the kinetic energy of Ar LMM Auger electron directly from the XAES spectra, it was approximately determined from the binding energies given in Table II. Assuming the Ar LMM transitions involve only Ar $2p_{3/2}$ and Ar 3p energy levels, the calculated kinetic energy values were found higher than the measured values given in Table IV only by about 0.5-1.0 eV. This confirms the correct assignment of the third Auger peak as the Ar LMM Auger transition.

There are two possible assignments for the second main peak in the XAES spectra of the sputtered a-C films. Considering the presence of oxygen in the oxidized surface of the x-ray generating target (the aluminum anode in this study), the second main peak may be identified as the C 1s XPS peak excited by the O Kα x-ray ($h\nu$ = 523 eV) with kinetic energy of ~240 eV.[24] However, this possibility is ruled out because x-ray monochromatic treatment was used in this study for the Al Kα x-ray source. In addition, the FWHM values of the second main peaks are in the range of 21.48-21.66 eV, typical of Auger transitions (Table IV), which is much higher than the FWHM values of the C 1s XPS spectra (in the range of 1.46-1.68 eV, Table II). Therefore, the second main peak is believed to be due to surface plasmon energy loss of C KLL Auger electrons leaving the surface at a kinetic energy of ~264.5 eV. This kind of surface plasmon energy loss for diamond and graphite is 22 and 28 eV, respectively.[12,13] From the data of Table IV, the kinetic energy difference between the first two main peaks (or surface plasmon energy loss) was calculated to be in the range of 20.9-21.3 eV (Table IV).

The surface plasmon energy loss is due to excitation of a surface plasma oscillation on the film surface when an Auger electron escapes through the surface layer, normally within 5-10 nm for a-C materials. This induces a loss in the kinetic energy of the escaped Auger electron equal to integer multiples of the plasmon energy that is a quantum of a plasma oscillation. Since a plasma oscillation in dielectric films is a collective longitudinal excitation of the valence electron gas, a volume plasmon energy can be determined as $h\omega_p/2\pi$, where h is Planck's constant and ω_p is the plasma frequency, given by $\omega_p^2 = ne^2/\varepsilon_0 m$,[30] where n is the electron concentration, e and m are the charge and rest mass of an electron, respectively, and ε_0 is the permittivity of free space. Alternatively, based on the approximation of semi-infinite plasma,[30] the frequency of a surface plasma oscillation ω_s is given by $\omega_s^2 = 0.5\omega_p^2$. Thus the surface plasmon energy, defined by $h\omega_s/2\pi$, is approximately equal to 0.707 $h\omega_p/2\pi$. Assuming that the density of the a-C film[2,5] is equal to 2.6 g/cm^3 and that all four valence electrons of the C atom contribute to the plasma oscillation upon excitation by a passing Auger electron, the electron concentration n and the plasma frequency ω_p can be estimated to be equal to 5.22×10^{29} m^{-3} and 4.08×10^{16} s^{-1}, respectively. Therefore, the volume plasmon energy and surface plasmon energy for an a-C film of density of 2.6 g/cm^3 can be calculated to be equal to 26.83 and 18.97 eV, respectively. Since the escape length of C KLL Auger electrons with kinetic energy of ~264.5 eV is about 2 nm,[31,32] the energy loss due to excitation of the plasma oscillation should be between 18.97 eV (surface plasmon energy) and 26.83 eV (bulk plasmon energy), which is in fair agreement with the kinetic energy loss values given in Table IV.

Based on the above theoretical analysis, it can be shown that the plasmon energy is proportional to the square root of the electron concentration, i.e., the film density. Hence, the plasmon energy increases with the film density. Figure 12 shows the variation of the film hardness and the binding energy

of Ar $2p_{3/2}$ electron with the kinetic energy difference between the first two main peaks in the C KLL Auger spectra, i.e., the energy loss due to excitation of surface plasma oscillation when a C KLL Auger electron leaves the a-C film surfaces. The obtained second-order polynomial function fit (with a correlation coefficient of 0.985) to the surface plasmon energy loss and film hardness data suggests that the density of the sputtered a-C films controls the nanohardness. Therefore, to increase the hardness, the deposition conditions must be optimized to produce carbon films of maximum density. The variation of the Ar $2p_{3/2}$ binding energy with the energy loss indicates that energetic Ar^+ ion bombardment during film deposition not only promotes film densification but also introduces a compressive residual stress in the films. However, a maximum compressive residual stress exists, which is associated with a stress relaxation mechanism involving a stress-induced phase transformation from sp^2 to sp^3 carbon hybridization, in accord with the discussion of the results shown in Fig. 9 presented in Sec. IIIC.

IV. CONCLUSIONS

Ultrathin a-C films synthesized by rf sputtering on Si(100) substrates were analyzed by XPS and XAES techniques to determine the effect of deposition conditions on the film compositions and carbon bonding structure and to elucidate the mechanisms responsible for the variation of the film nanohardness. Based on the presented results and discussion, the following main conclusions can be drawn.

1. Small amounts of argon, oxygen, and nitrogen were detected in the a-C films. The presence of Ar is attributed to incorporation or implantation processes, and its concentration depends on the intensity of Ar^+ ion bombardment during deposition. Nitrogen is either physically or chemically adsorbed on the freshly grown carbon film surfaces at the end of the deposition process. The small amounts of oxygen in the bulk of the films (1-2 at%) are due to various sources and can be reduced by

energetic ion bombardment during film growth. The argon and oxygen contents do not exhibit any direct effects on the nanohardness of the films.

2. The Ar content of the a-C films yields important insight into the plasma environment in the vicinity of the growing film surface, while the binding energy of core level Ar 2p XPS transitions provides information about the mechanical environment in the a-C films (e.g., residual compressive stress due to energetic ion bombardment during deposition). The nearly same binding energy shifts of both the core level Ar 2p transitions and the valence band transitions Ar 3s and Ar 3p of embedded Ar atoms suggest that noble atoms (such as Ar) reveal only the mechanical environments in the a-C films, such as residual stress field and crystal field (short range for amorphous materials).
3. From the analysis of the C 1s XPS spectra, the sputtered a-C films were found to be rich in sp^2 hybridized carbon. For a-C films of hardness between 19 and 40 GPa, the sp^3 carbon content is in the range of 22-28%, depending on the intensity of Ar^+ bombardment during sputtering. Material densification due to energetic ion bombardment promotes the formation of sp^3 carbon, as evidenced by the increase of the sp^3 carbon content with the Ar concentration in the a-C films. The interdependence of the sp^3 carbon fraction, Ar content, and binding energy of Ar 2p reveals a stress-induced phase transformation from sp^2 to sp^3 carbon hybridization in a-C films exhibiting high compressive residual stresses.
4. The three main peaks in the XAES spectra of the a-C films were identified as C KLL Auger peak (~264.5 eV), C KLL Auger peak (~243.3 eV) shifted due to the surface plasmon energy loss, and Ar LMM Auger peak (~222.0 eV). The variation of the a-C film nanohardness with the surface plasmon energy loss reveals a direct correlation between the density (rather than the apparent sp^3 carbon content) and the hardness of the films. This is because the plasmon energy loss increases

with the concentration of electron gas in the a-C films (i.e., film density). This finding suggests that in order to increase the hardness of the sputtered a-C films, the deposition conditions must be optimized to produce maximum-density films.

Acknowledgments

This research was supported by the Surface Engineering and Tribology Program of the National Science Foundation under Grant No. CMS-9734907 and the Computer Mechanics Laboratory at the University of California at Berkeley. The authors are grateful to Dr. S. W. Yeh from Chevron Chemical Co., Richmond, California, for obtaining the XPS and XAES spectra.

References

[1]Y. Lifshitz, in *The Physics of Diamond*, edited by A. Paoletti and A. Tucciarone (IOS, Amsterdam, The Netherlands, 1997), pp. 209-253.

[2]J. Schwan, S. Ulrich, H. Roth, H. Ehrhardt, S. R. P. Silva, J. Robertson, R. Samlenski, and R. Brenn, J. Appl. Phys. **79**, 1416 (1996).

[3]J. Schwan, S. Ulrich, T. Theel, H. Roth, H. Ehrhardt, P. Becker, and S. R. P. Silva, J. Appl. Phys. **82**, 6024 (1997).

[4]W. Lu and K. Komvopoulos, J. Appl. Phys. **85**, 2642 (1999).

[5]W. Lu and K. Komvopoulos, J. Appl. Phys. **86**, 2268 (1999).

[6]W. Lu, K. Komvopoulos, and S. W. Yeh, J. Appl. Phys. **89**, 2422 (2001).

[7]J. Schwan, S. Ulrich, V. Batori, H. Ehrhardt, and S. R. P. Silva, J. Appl. Phys. **80**, 440 (1996).

[8]J. W. Ager III and M. D. Drory, Phys. Rev. B **48**, 2601 (1993).

[9]W. Lu and K. Komvopoulos, Appl. Phys. Lett. **76**, 3206 (2000).

[10]K. S. Kim and N. Winograd, Chem. Phys. Lett. **30**, 91 (1975).

[11]J. Diaz, G. Paolicelli, S. Ferrer, and F. Comin, Phys. Rev. B **54**, 8064 (1996).

[12]Y. Mizokawa, T. Miyasato, S. Nakamura, K. M. Geib, and C. W. Wilmsen, Surf. Sci. **182**, 431 (1987).

[13]Y. Mizokawa, T. Miyasato, S. Nakamura, K. M. Geib, and C. W. Wilmsen, J. Vac. Sci. Technol. A **5**, 2809 (1987).

[14]J. C. Lascovich, R. Giorgi, and S. Scaglione, Appl. Surf. Sci. **47**, 17 (1991).

[15]J. C. Lascovich, and S. Scaglione, Appl. Surf. Sci. **78**, 17 (1994).

[16]W. Lu and K. Komvopoulos, J. Tribol. **123,** 641 (2001).

[17]D. A. Shirley, Phys. Rev. B **5**, 4709 (1972).

[18]P. Sherwood, in *Practical Surface Analysis by Auger and X-ray Photoelectron Spectroscopy*, edited by D. Briggs and P. Seah (Wiley, New York, NY, 1983), p. 445.

[19]S. T. Jackson and R. G. Nuzzo, Appl. Surf. Sci. **90**, 195 (1995).

[20]D. Marton, K. J. Boyd, A.H. Al-Bayati, S.S. Todorov, and J. W. Rabalais, Phys. Rev. Lett. **73**, 118 (1994).

[21]H. Sjostrom, L. Hultman, J.-E. Sundgren, S. V. Hainsworth, T.F. Page, and G. S. A. M. Theunussen, J. Vac. Sci. Technol. A **14**, 56 (1996).

[22]S. Souto, M. Pickholz, M.C. dos Santos, and F. Alvarez, Phys. Rev. B **57**, 2536 (1998).

[23]F. R. McFeely, S. P. Kowalczyk, L. Ley, R. G. Cavell, R. A. Pollak, and D. A. Shirley, Phys. Rev. B **9**, 5268 (1974).

[24]J. C. Lascovich and A. Santoni, Appl. Surf. Sci. **103**, 245 (1996).

[25]B. Chapman, *Glow Discharge Processes: Sputtering and Etching* (Wiley, New York, NY, 1980).

[26]M. Konuma, *Film Deposition by Plasma Techniques* (Springer, Berlin, Germany, 1992).

[27]M. A. Lieberman and A. J. Lichtenberg, *Principles of Plasma Discharges and Materials Processing* (Wiley, New York, NY, 1994).

[28]C. A. Davis, *Thin Solid Films*, **226**, 30 (1993).

[29]*Tables of Physical and Chemical Constants and Some Mathematical Functions*, compiled by G. W. C. Kaye and T. H. Laby (Longman, New York, NY, 1986), p. 311.

[30]C. Kittel, *Introduction to Solid State Physics*, 4th ed. (Wiley, New York, NY, 1971).

[31]G. C. Smith, *Quantitative Surface Analysis for Materials Science*, The Institute of Metals, 1991.

[32]J. F. Watts, *Introduction to Surface Analysis by Electron Spectroscopy* (Oxford University Press, New York, NY, 1990).

Table I. Deposition conditions, properties, and composition of ultrathin a-C films deposited on Si(100) substrates by rf sputtering.

Sample	Deposition conditions[a]			Film properties					Film composition[b]				
	P (W)	V_s (V)	t (min)	d (nm)	σ (nm)	H_{eff} (GPa)	$[E/(1-\nu^2)]_{eff}$ (GPa)	h_c/d	C (at%)	Ar (at%)	O (at%)	N (at%)	Si (at%)
E	500	0	5	22	0.38	20.44	142.8	0.23	87.92	1.30	9.98	0.94	0.07
I	500	-100	5	14	0.18	26.12	185.77	0.28	88.70	1.51	8.72	0.90	0.17
C	500	-200	5	11	0.17	29.08	184.56	0.31	90.07	1.63	7.31	0.91	0.01
F	500	-200	10	39	0.15	34.33	219.07	0.07	90.11	2.03	7.49	0.67	0.00
J	500	-300	5	13	0.17	28.56	190.96	0.34	89.99	1.90	7.01	0.90	0.06
B	750	0	5	27	0.90	19.67	132.61	0.19	89.09	0.51	10.69	0.75	0.01
H	750	-100	5	22	0.18	34.20	197.69	0.16	90.29	1.71	7.28	0.46	0.26
A	750	-200	5	10	0.20	39.19	185.10	0.23	89.78	1.93	7.39	0.95	0.05
D	750	-200	10	69	0.15	31.83	207.52	0.04	90.19	1.54	7.44	0.88	0.01
G	750	-300	5	17	0.19	19.84	133.19	0.39	88.79	2.07	8.15	1.02	0.00

[a]Ar gas flow rate = 20 sccm; working pressure = 3 mTorr.

[b]The elemental composition was determined by XPS without cleaning the sample surfaces, on which significant amounts of oxygen were adsorbed from the ambient.[6]

Table II. Binding energy (BE) of core level XPS transitions C 1s and Ar $2p_{3/2}$ with full width at half magnitude (FWHM) values, and valence band transitions Ar 3p and Ar 3s of different a-C films.

Sample	Core level transitions (eV)				Valence band transitions (eV)	
	C 1s		Ar $2p_{3/2}$		Ar 3p	Ar 3s
	BE	FWHM	BE	FWHM	BE	BE
B	284.5	1.49	242.1	1.03	9.65	22.93
A	284.4	1.68	241.5	1.03	9.37	22.47
D	284.3	1.59	241.3	1.06	9.22	22.35
E	284.5	1.46	241.9	1.04	9.59	22.82
C	284.3	1.56	241.4	1.06	9.21	22.38
F	284.4	1.68	241.5	1.01	9.39	22.49

Table III. Binding energy (BE) and atomic percentages of characteristic Gaussian peaks used to fit the core level C 1s XPS spectra, atomic percentage of carbon, and sp^3 carbon content of different a-C films.

Feature	a-C Sample											
	B		A		D		E		C		F	
	BE (eV)	at%	BE (eV)	at%	BE (eV)	at%	BE (eV)	at%	BE (eV)	at%	BE (eV)	at%
C 1s (1)	284.45	59.13	284.38	57.05	284.23	57.06	284.44	55.84	284.28	57.35	284.39	56.79
C 1s (2)	285.47	15.30	285.44	18.86	285.33	18.04	285.45	17.26	285.37	17.89	285.37	19.96
C 1s (3)	286.69	6.88	286.69	6.40	286.73	7.57	286.75	8.00	286.73	6.91	286.71	7.38
C 1s (4)	288.12	4.67	288.11	4.27	288.37	4.32	288.42	4.42	288.25	4.48	288.39	3.72
C 1s (5)	289.56	2.02	289.64	2.06	290.11	2.19	290.12	1.70	289.92	2.32	290.05	1.54
C 1s (6)	291.20	1.09	291.37	1.14	291.87	1.02	291.79	0.69	291.69	1.13	291.72	0.72
C (at%)	89.09		89.78		90.19		87.92		90.07		90.11	
sp^3 (%)	23.64 ±1.08		27.04 ±0.31		25.91 ±0.31		25.45 ±0.10		26.09 ±0.70		27.08 ±0.64	

Table IV. Kinetic energy (KE) and full width at half magnitude (FWHM) of decomposed main Auger transitions in the C KLL Auger spectra and kinetic energy difference (ΔE) between C KLL and A2 Auger transitions (surface plasmon energy loss) of different a-C films.

Sample	C KLL		A2		Ar LMM		ΔE (eV)
	KE (eV)	FWHM (eV)	KE (eV)	FWHM (eV)	KE (eV)	FWHM (eV)	
B	263.93	19.51	243.03	21.66	222.33	19.76	20.90
A	264.74	19.83	243.45	21.57	222.05	19.87	21.30
D	264.55	19.74	243.34	21.50	222.30	19.91	21.21
E	264.24	19.23	243.32	21.59	221.79	19.94	20.92
C	264.45	19.81	243.33	21.62	221.73	19.96	21.12
F	264.63	19.81	243.37	21.48	222.05	19.83	21.26

List of Figures

Fig. 1. (a) Entire XPS spectrum typical of a-C film (sample A) illuminated by Al Kα x-ray, (b) integral C KLL Auger (XAES) spectrum (plotted in binding energy scale) with three Gaussian fits after Shirley background subtraction, and (c) valence band XPS spectrum.

Fig. 2. Effect of energetic ion bombardment (bias voltage) and rf power on oxygen content of a-C films.

Fig. 3. Effect of substrate bias voltage on Ar content of a-C films deposited in 5 min under rf power of 500 and 750 W.

Fig. 4. Effect of rf power and deposition time on Ar content of a-C films deposited under substrate bias voltage of –200 V.

Fig. 5. Variation of a-C film nanohardness with (a) Ar content and (b) binding energy of Ar $2p_{3/2}$ XPS transition.

Fig. 6. XPS spectra of (a) core level Ar 2p transitions and (b) Ar 3s and (c) Ar 3p valence band transitions of a-C films (samples A-F).

Fig. 7. Comparison of binding energy shifts of core level Ar $2p_{3/2}$ and valence band Ar 3s and Ar 3p transitions of a-C films (samples A-F) referred to those of (a) free Ar atoms and (b) embedded Ar atoms in the a-C film of sample B.

Fig. 8. Decomposition of a typical core level C 1s XPS spectrum of a-C film (sample A).

Fig. 9. Variation of *sp*3 carbon content in a-C materials and binding energy of Ar $2p_{3/2}$ with Ar content of a-C films (samples A-F).

Fig. 10. Relation between *sp*3 carbon content in a-C materials and nanohardness of a-C films (samples A-F).

Fig. 11. First-order derivative XAES spectra (plotted in binding energy scale) of a-C films deposited under zero (sample B) and –200 V (sample A) bias voltage.

Fig. 12. Variation of nanohardness and Ar $2p_{3/2}$ binding energy with surface plasmon energy loss of a-C films (samples A-F).

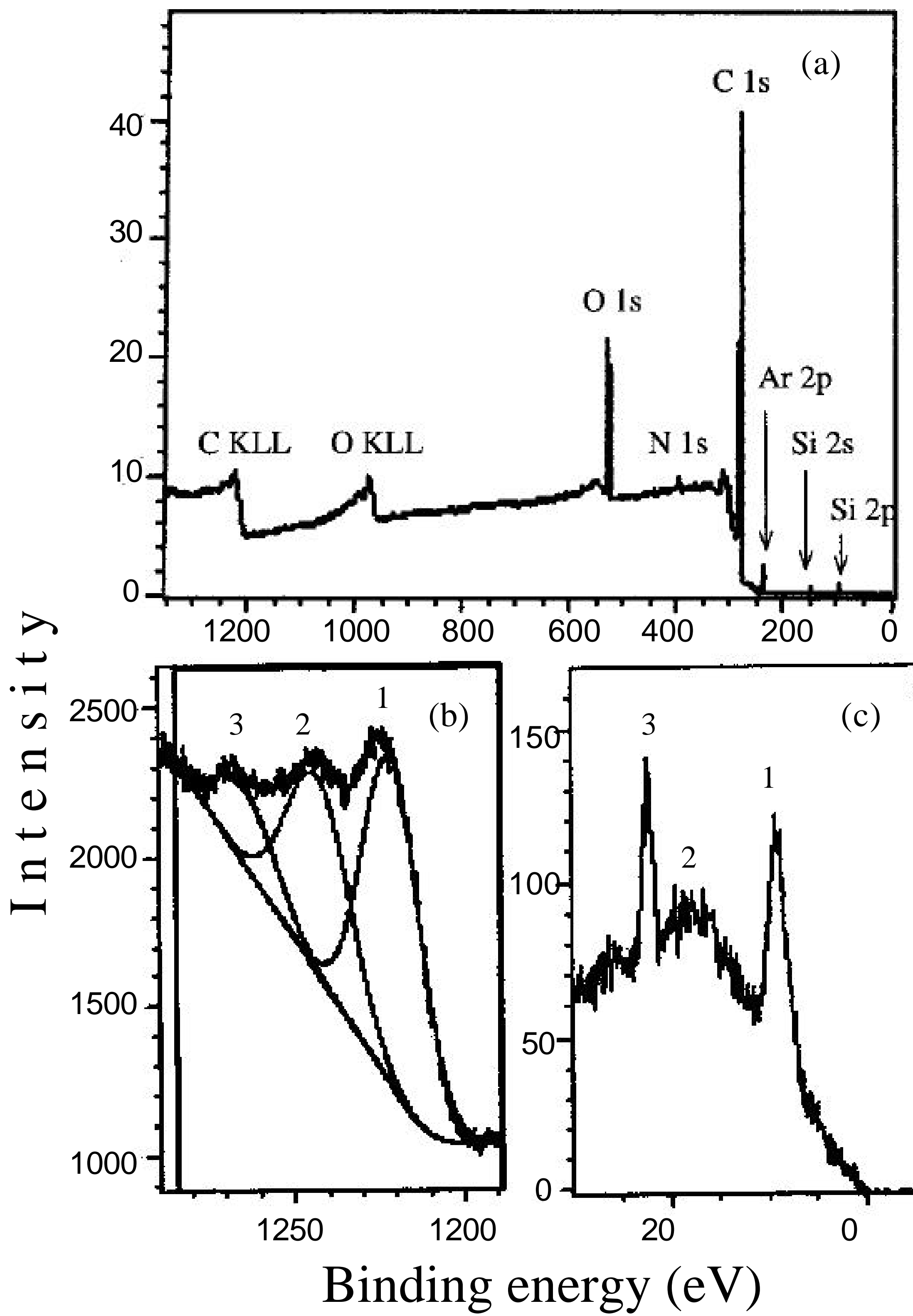

Figure 1

(a t %

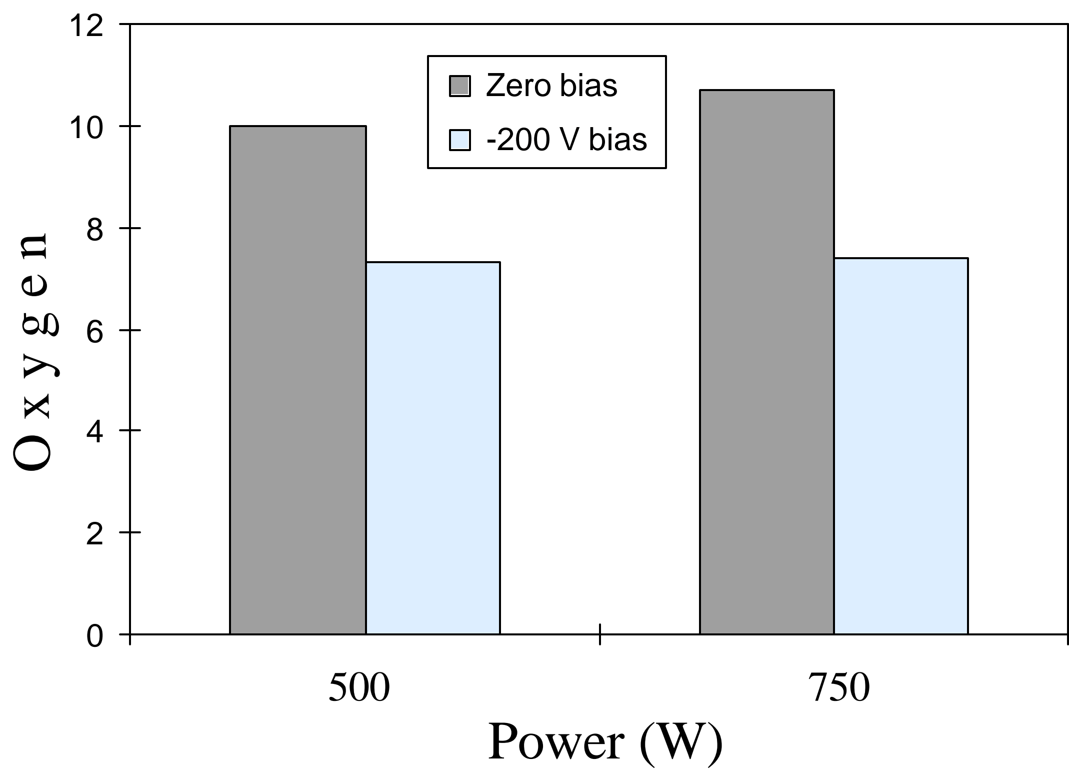

Figure 2

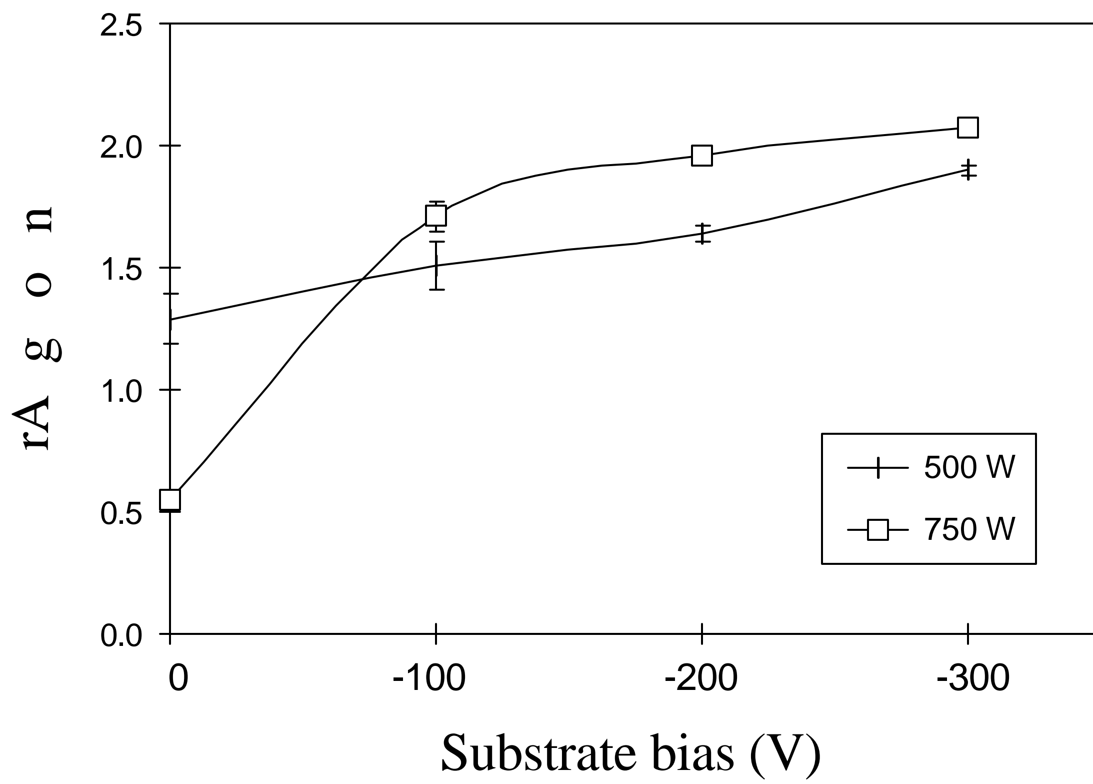

Figure 3

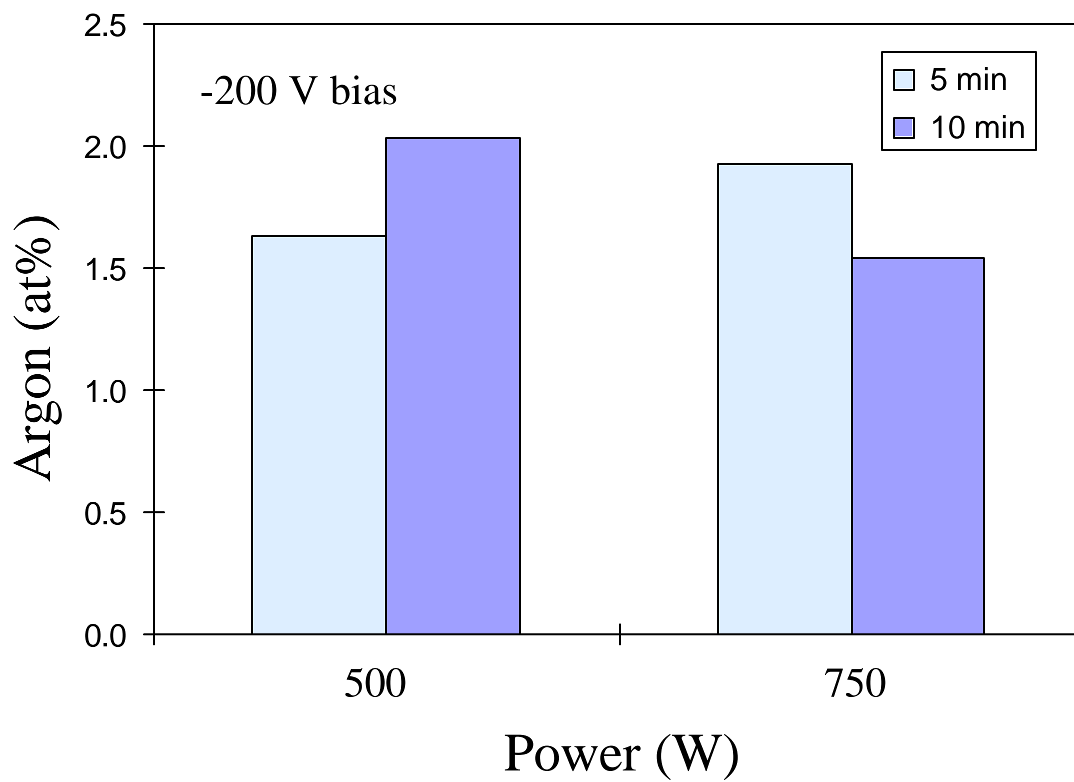

Figure 4

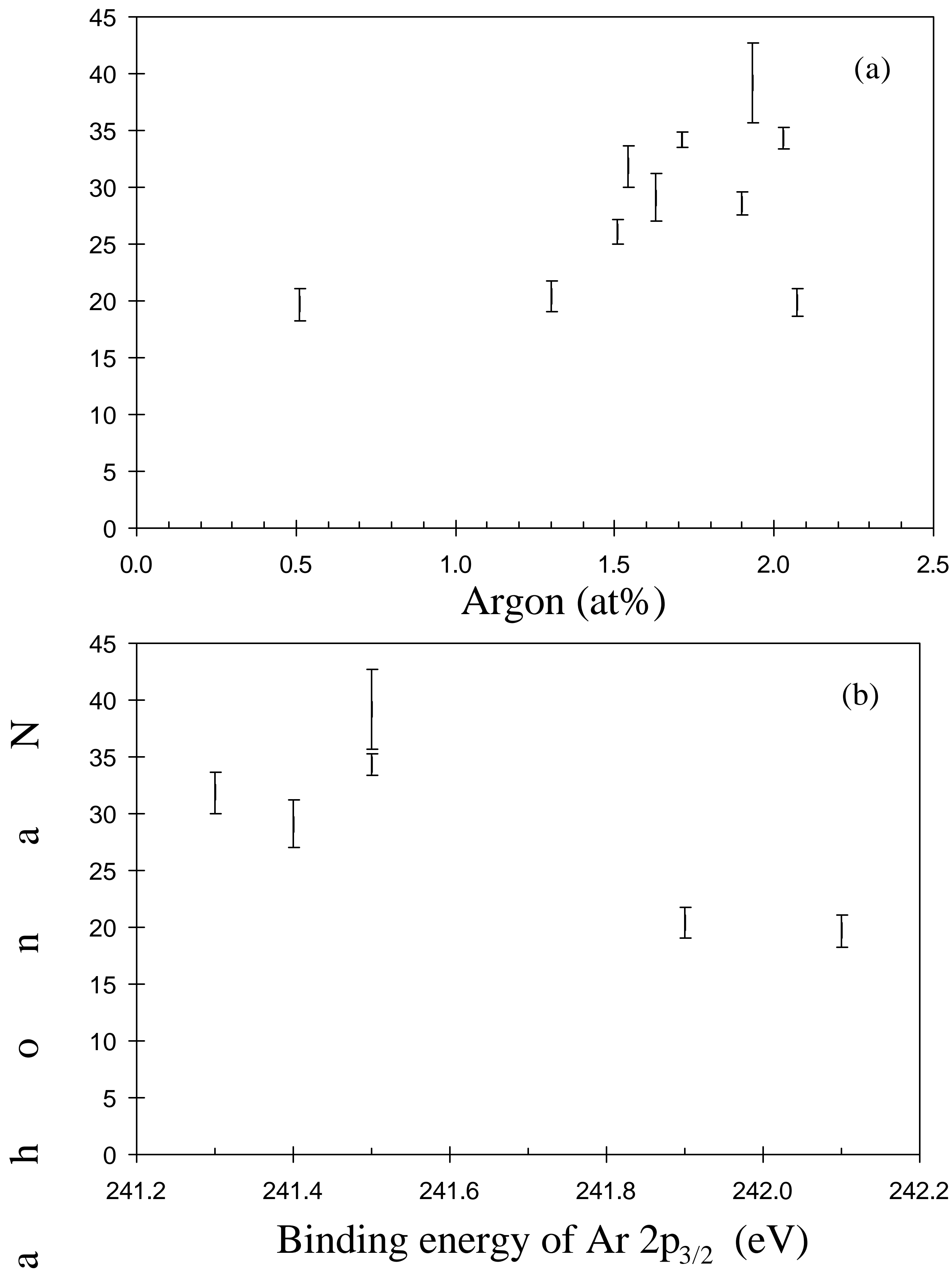

Figure 5

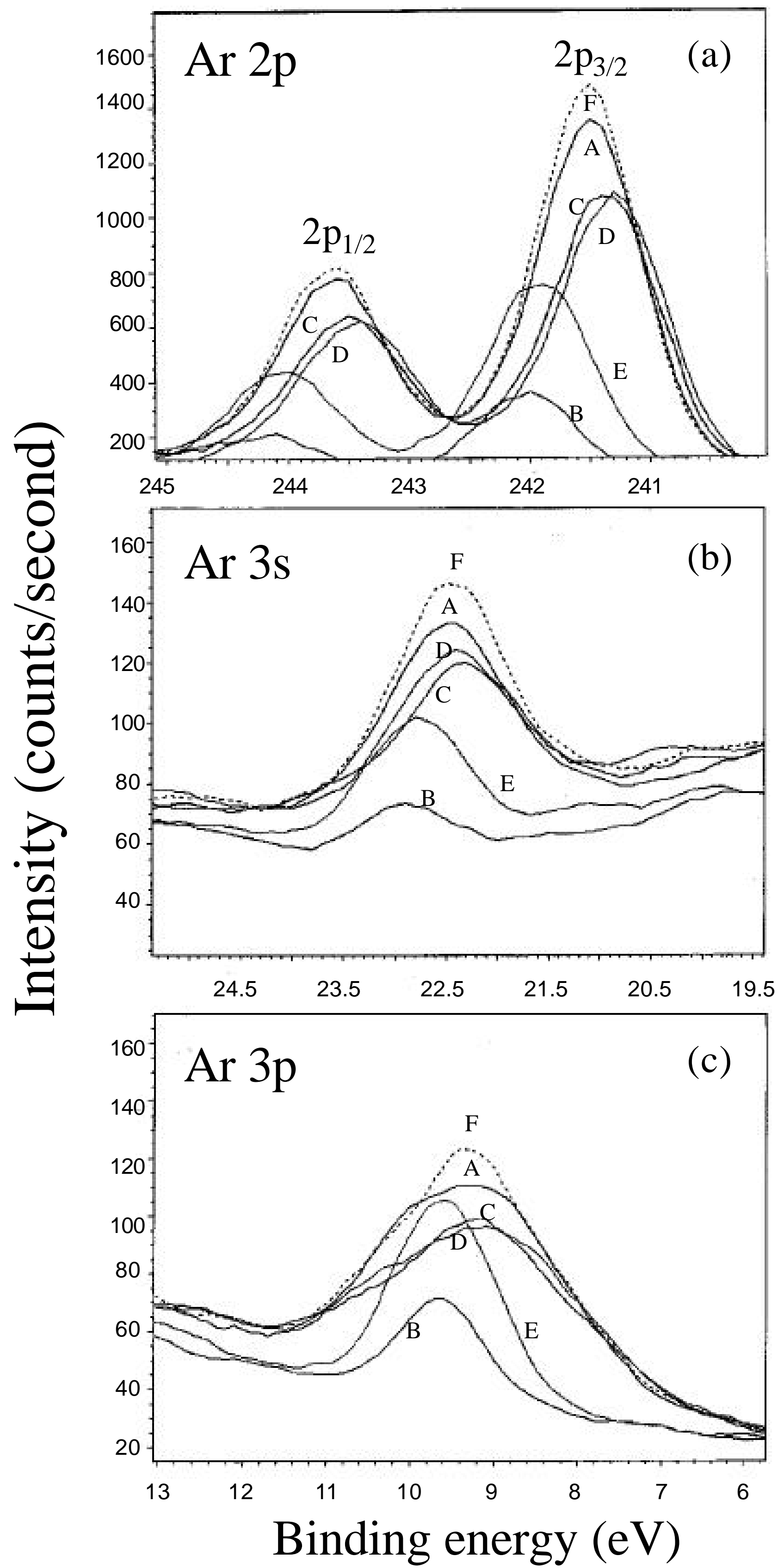

Figure 6

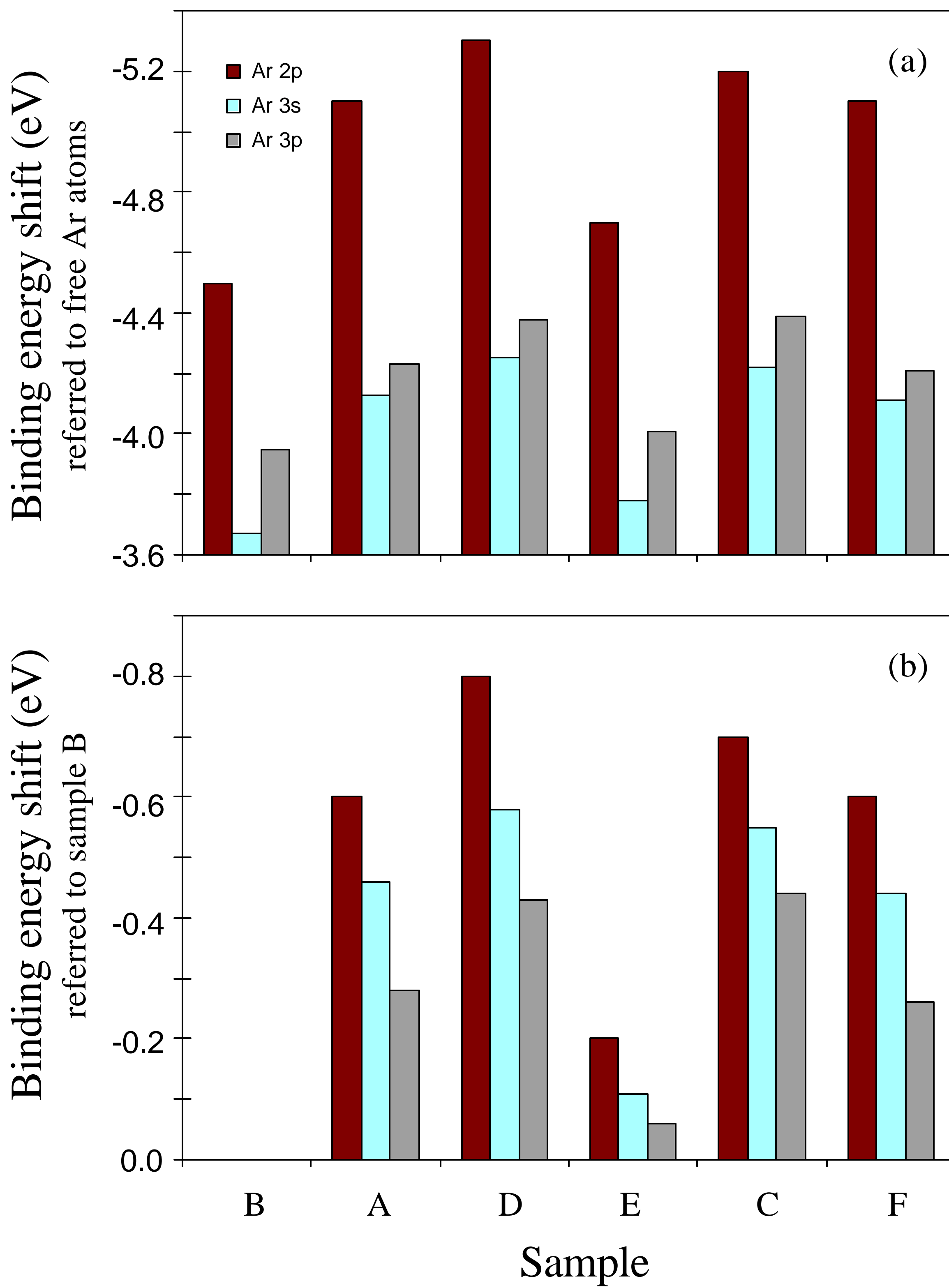

Figure 7

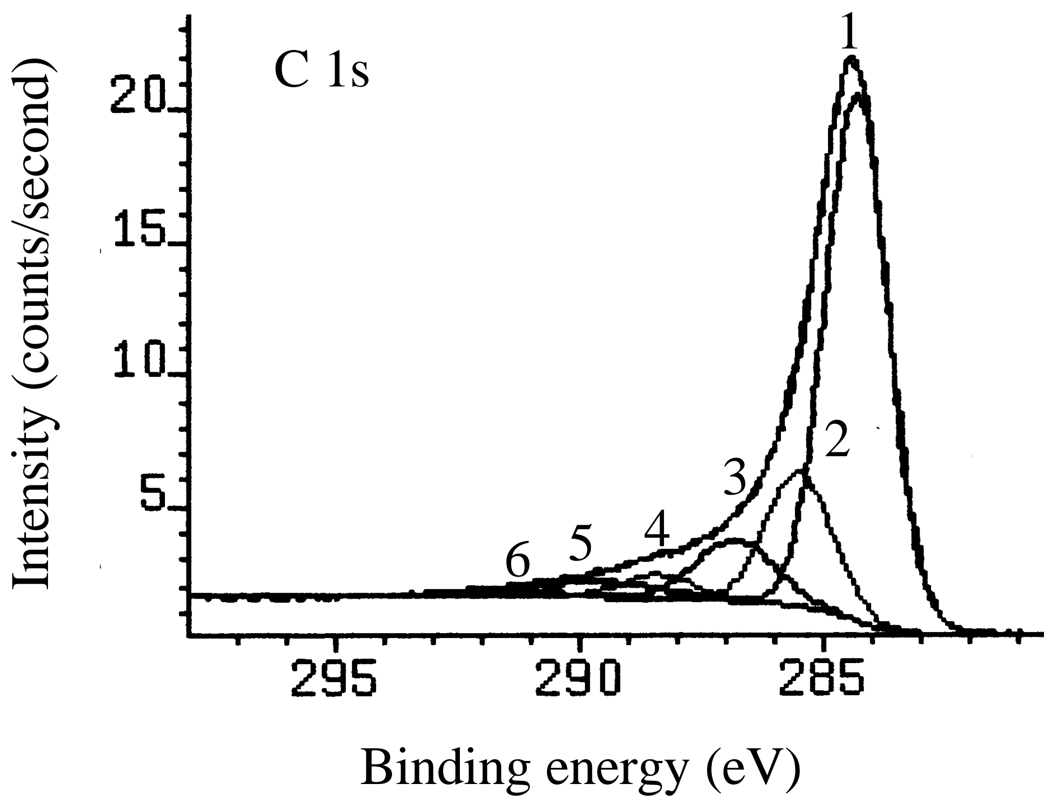

Figure 8

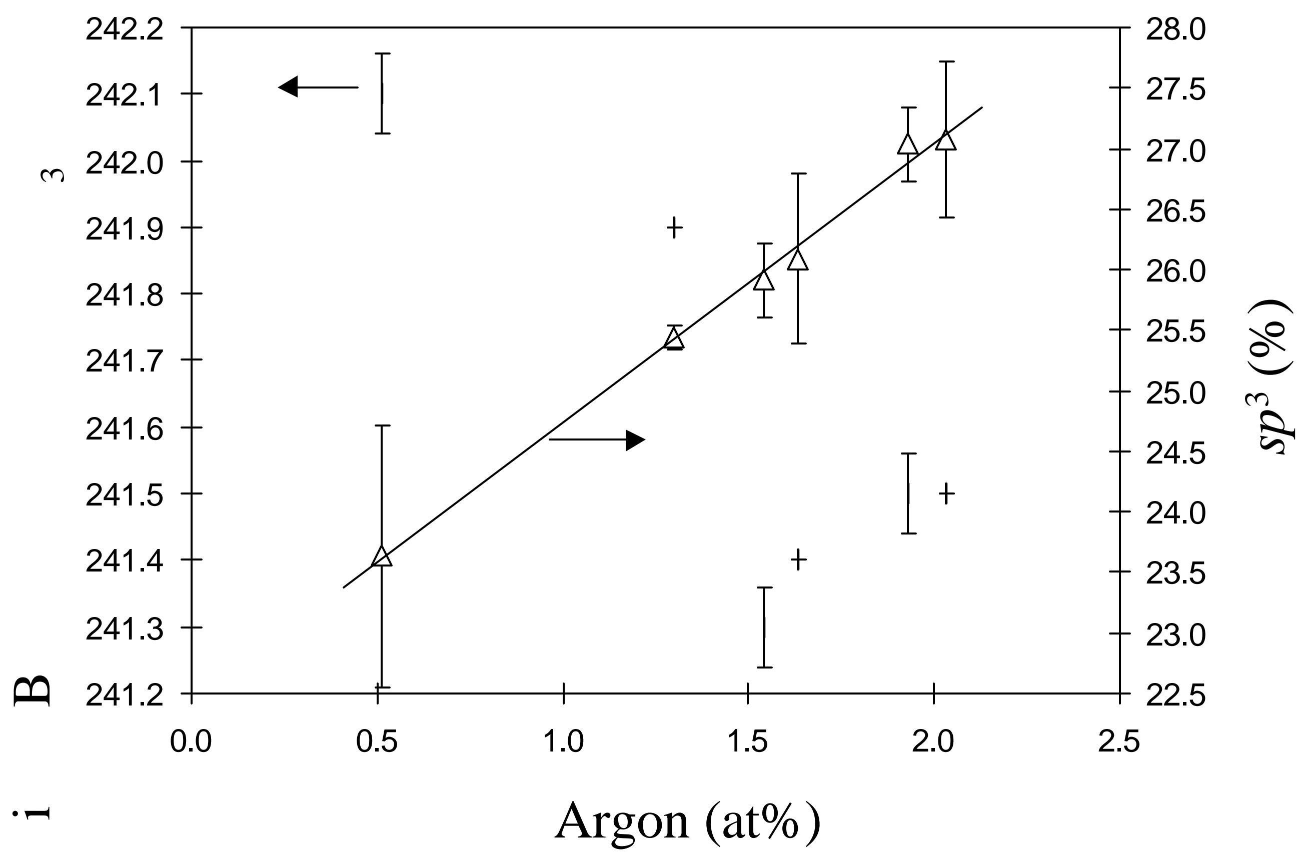

Figure 9

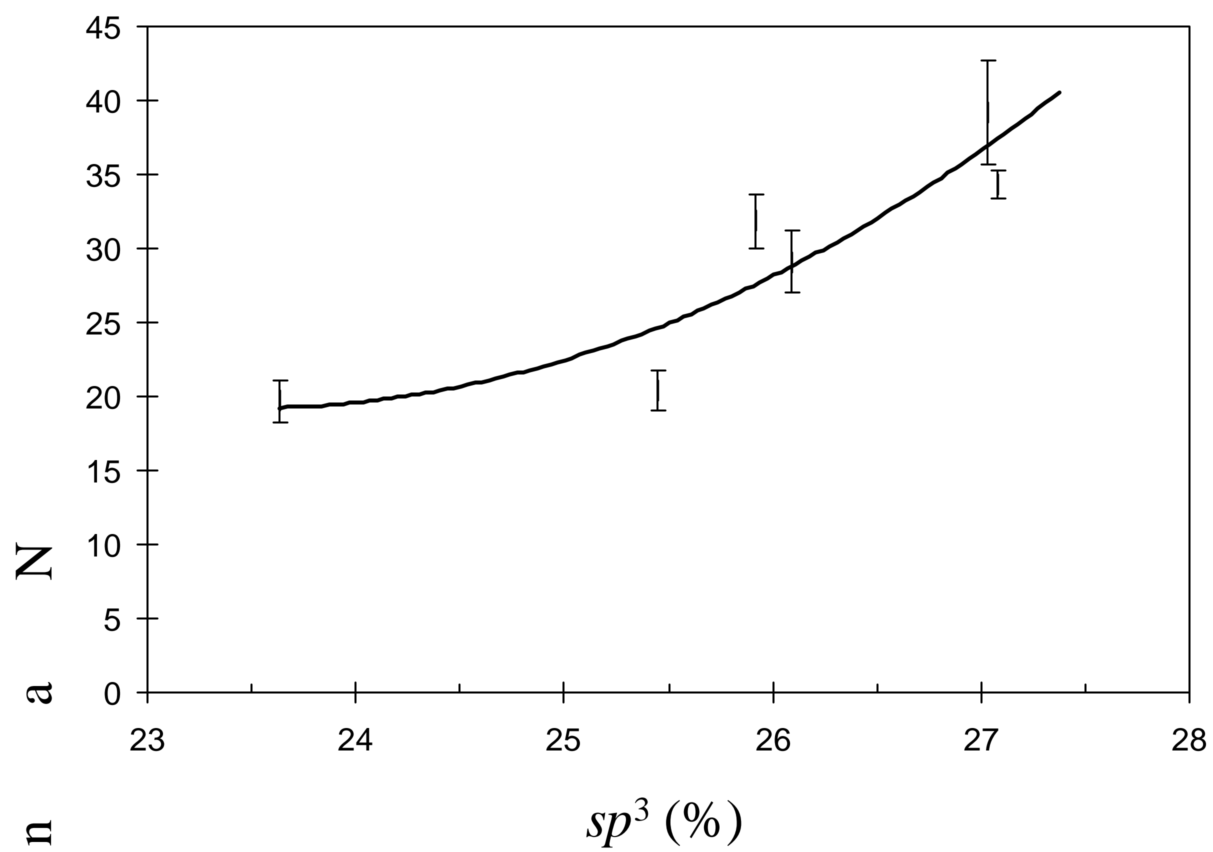

Figure 10

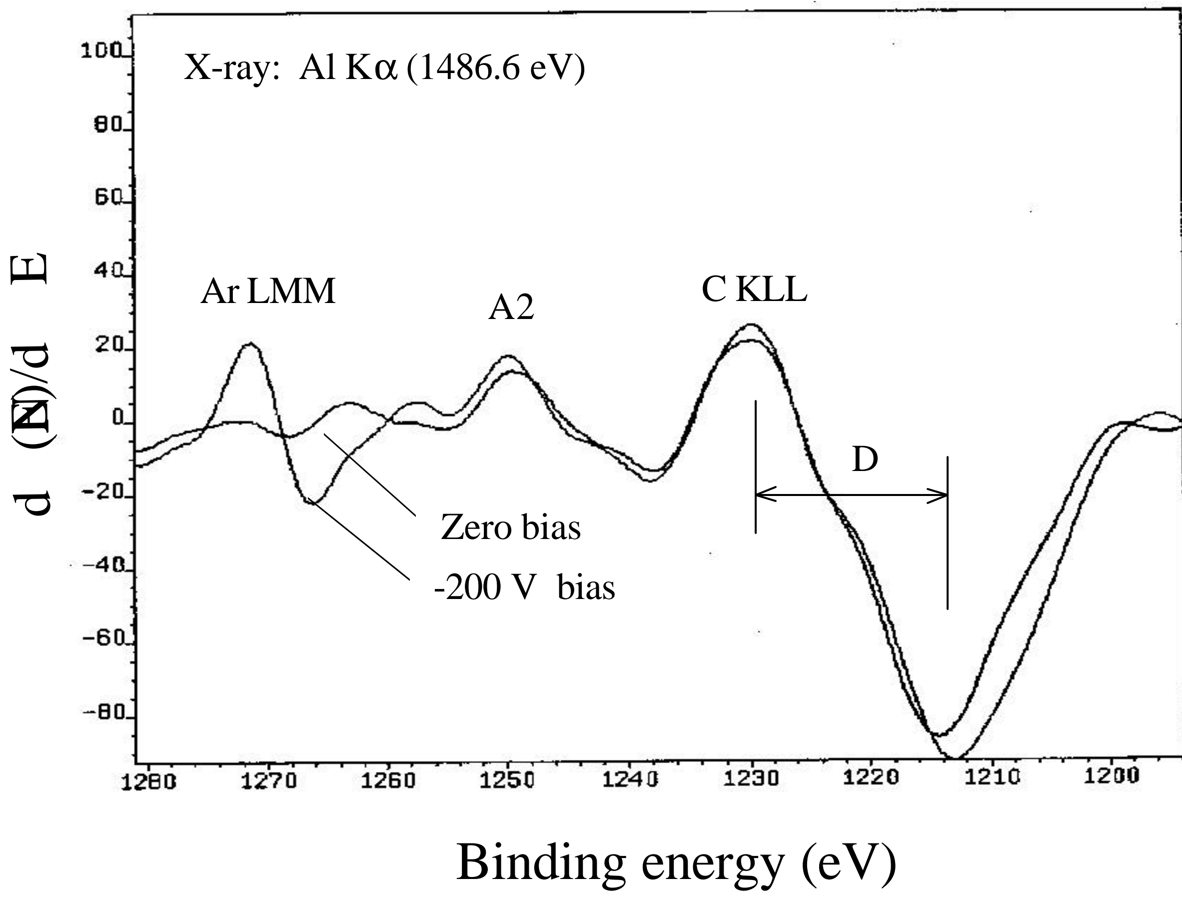

Figure 11

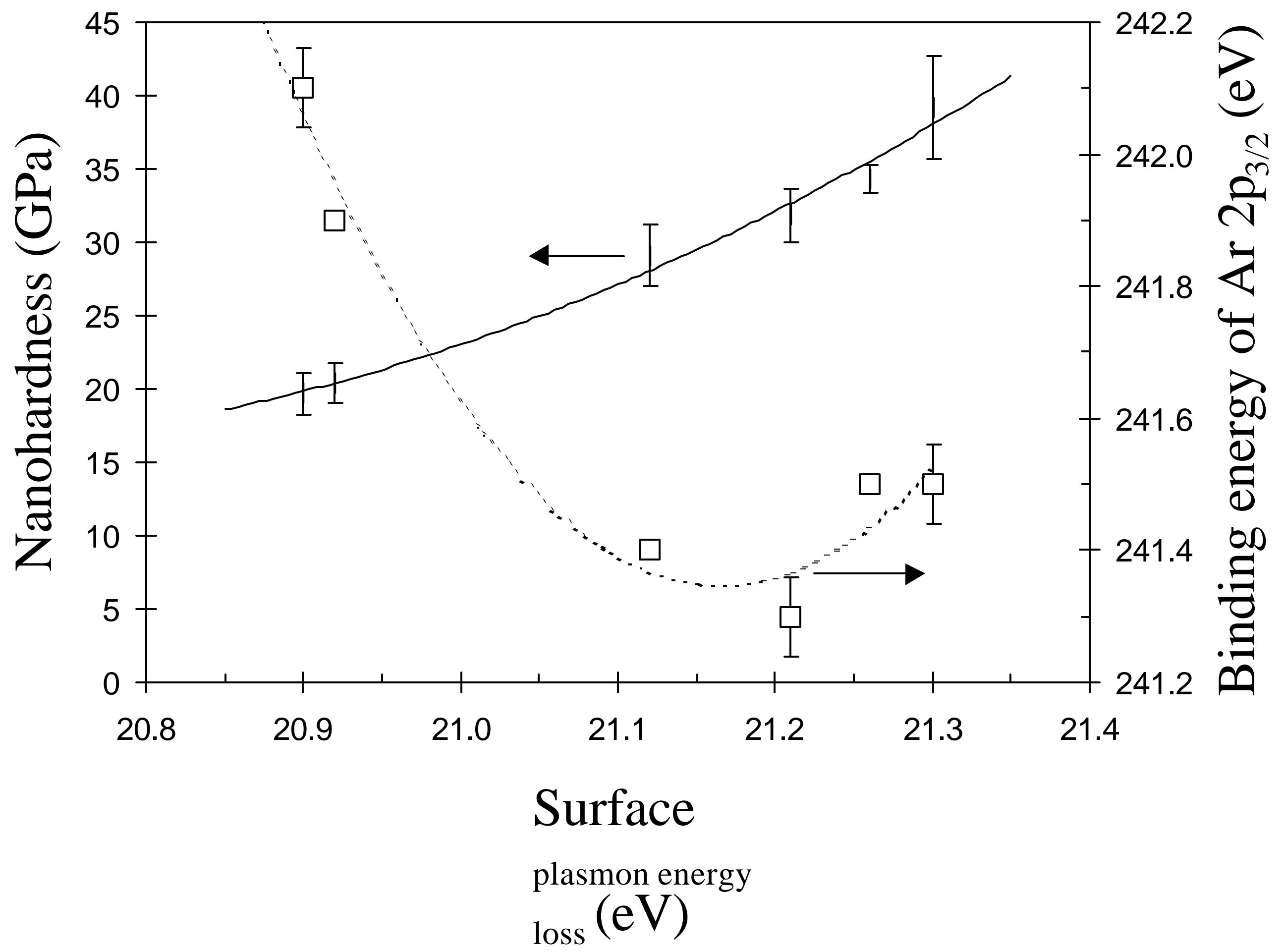

Figure 12